Chapter 4

LOW-DENSITY MgAlMnFeCu HIGH ENTROPY ALLOY

This chapter deals with the synthesis and phase evolution study of low-density MgAlMnFeCu high entropy alloy through mechanical alloying (MA) followed by spark plasma sintering (SPS). Significant progress has been made in studying HEAs based on the transition series elements with and without the addition of Al [19,114]. Although Mg is the lightest and cost-effective element available for structural applications, there is only limited literature on its effect on the HEAs [115–123]. Considerable efforts were made by Li *et al.* [121,124] to study the impact of Mg addition in the $Mg_x(MnAlZnCu)_{100-x}$ (x = 20, 33, 43, 45.6, 50 at%) HEAs on their microstructures, bulk densities and mechanical properties. The as-cast HEA prepared by induction melting had an HCP structure with Al-Mn based icosahedral precipitates embedded in the matrix. These Mg-based HEAs exhibited low density in the range from 4.29 g cc^{-1} to 2.20 g cc^{-1}, high hardness (4.29 to 1.78 GPa) and high compressive strength (from 500 to 400 MPa) at room temperature. However, the failure strain of these HEAs was in the range of ~ 3-5%. These HEAs have excellent thermal stability. In particular, the $Mg_{20}(MnAlZnCu)_{80}$ HEA has shown very good thermal stability up to 677 ˚C (950 K). Chen *et al.* [123] reported the formation of amorphous phases during mechanical alloying (MA) of BeMgTiCo and BeMgTiCoZn HEAs with all HCP elements. In another investigation, Youssef *et al.* [117] reported the formation of lightweight single-phase FCC structure in $Al_{20}Li_{20}Mg_{10}Sc_{20}Ti_{30}$ HEA subjected to MA for 16 h. The MA leads to the formation of nanocrystalline HEA with grain size and hardness of ~12 nm and ~5.8 GPa, respectively. After annealing at 500 ˚C (773 K) for 1h, these alloys had appreciable grain growth to 26 nm and hardness up to 4.9

GPa. During annealing, these HEAs transformed from FCC to HCP structure with *c*/*a* ratio of 1.588.

Sanchez *et al.* [125] reported the formation of low-density HEA (LDHEA) by die casting in $Al_{60}Cu_{10}Fe_{10}Cr_5Mn_5Ni_5Mg_5$ alloy having low density (4.6 g cc^{-1}) and high hardness of 9.16 GPa. The high values of microhardness in these LDHEAs are due to the formation of complex intermetallics during die casting. Senkov et al. [126,127] reported TiVCrZrNb low density refractory high entropy alloy (6.57 g cc^{-1}) having high yield strength at room temperature (1298 MPa) and at 1000 °C (259 MPa). Stepanov et al. [128,129] prepared lightweight AlTiVNb (5.59 g cc^{-1}) quaternary high entropy alloy having a single BCC phase. The prepared alloy exhibited a compressive yield strength of 1020 MPa at room temperature and 685 MPa at 800 °C. Kumar and co-workers [130–132] made significant efforts in studying the effect of Mg addition in the HEA formation. Maulik and Kumar [131] reported the formation of HEAs with two phases during the mechanical alloying of $AlFeCuCrMg_x$ (x = 0, 0.5, 1.0, 1.7 at%). The alloys AlCrFeCu and $AlFeCuCrMg_{0.5}$ subjected to MA for 20 h form a major BCC phase with a minor FCC phase. Similarly, AlMgCrFeCu and $AlFeCuCrMg_{1.7}$ alloys were observed to contain two BCC phases. The dynamic DSC thermogram confirms the thermal stability of these alloys up to 500 ˚C (773 K). Maulik and Kumar [132] reported the detailed structural evolution of phases during spark plasma sintering (SPS) of these Mg-based HEAs. They observed the formation of AlFe, $MgCu_2$ and Mg_2Cu along with the disordered BCC phase. However, the phase fraction of the intermetallic phases was dependent on the composition of the HEAs. The AlFe was the primary phase for $AlFeCuCrMg_{1.7}$ HEA SPSed at 800 ˚C along with the other minor phases, i.e., $MgCu_2$ and Mg_2Cu. Kanchandani *et al.* [133] carried out MA of $AlMgFeCuCrNi_{4.75}$ alloy for 20 h for the synthesis of nanocrystalline HEA with BCC (major) and FCC (minor) phases. They have

also reported the effect of sintering at 900 ˚C on the phase evolution of these HEAs. After sintering, the BCC and FCC phases transform into Ni_3Al type ordered phase having an excellent hardness of 4.24 GPa, which is higher than that of INCONEL 718. Li *et al.* [119] attempted to develop CaMgZnSrYb HEA-bulk metallic glass for a biomedical application having superior mechanical properties and better corrosion resistance compared to their conventional counterparts.

In the present work, MA was used for the synthesis of MgAlMnFeCu HEA. The MA is the most preferred technique in this case, as the positive enthalpy of mixing between individual elements, as can be seen from calculations based on the Miedema model [45], may result in segregation or clustering in as-cast samples. The effect of Mg addition on phase evolution in this HEA was studied carefully through XRD and TEM. A detailed investigation was carried out to study the phase evolution after SPS of MgAlMnFeCu HEA. The effect of Mg addition on solid solution formation was discussed based on thermodynamical calculations, i.e., parametric approach and CALPHAD.

4. Results

4.1. Phase prediction of chosen alloy along temperature scale using CALPHAD

Figure 4.1 displays amount of phase evolved as a function of temperature. From the figure it can be easily understood that the liquidus temperature of the alloy is ~1327 °C (1600 K). The nucleation and growth of BCC_B2 phase start at the liquidus point. Two more phases (Cubic_A13 and Laves_C15 phase) precipitate from the liquid phase forming a mixture of three solid phases and a liquid phase. The remaining liquid phase solidifies to $CuMg_2$ type cubic Laves phase. The single point equilibrium calculations were done at various temperatures to understand the compositional variation in phases as a function of temperature. The composition of the phases at three different temperature are displayed in **Table 4.1**. From the table one can depict that BCC_B2 phase is Fe-rich

containing Mn and Al. While the Cubic_A13 phase is Mn-rich having small amount of Fe and Al. $CuMg_2$ phase is a cubic AB_2 type stoichiometric phase, while Laves_C15 phase is $MgCu_2$ type cubic phase.

4.2. Characterization of as-milled MgAlMnFeCu HEA

Figure 4.2 shows the phase evolution during MA of MgAlMnFeCu HEA for different milling periods up to 60 h. The diffraction peaks corresponding to all alloying elements in the pre-mixed powders can be predominantly observed. The peak intensities corresponding to various elements are different due to variations in the atomic scattering factor of each component in the HEA. Milling for 5 h leads to the broadening of peaks and reduction in the diffraction intensities corresponding to all the elements. Further, the peak corresponding to (002) reflection of Mg disappears. Milling for 10 h leads to the disappearance of all the reflections corresponding to Mg, while the intensity of peaks corresponding to (111), (220) and (311) reflections of Al, and (111) reflections of Cu decreases significantly. It was observed that the diffraction peaks corresponding to Mg disappear earlier than those corresponding to the other elements. The intensity of the peak corresponding to (111) reflection of Cu further decreases while the high angle diffraction peaks of Cu corresponding to the (220), (311) and (222) reflections disappear after 20 h of milling. Further, milling of the MgAlMnFeCu HEA up to 30 h leads to the complete dissolution of Cu in the solid solution. After 30 h of milling, all the diffraction peaks could be indexed done to a BCC phase, which is quite proximate with the α-Fe; and a γ-brass type of phase (quite similar to the α-Mn). Milling up to 60 h of duration was carried out in order to study further transformations in BCC and γ-brass type phases, which may lead to the formation of a single-phase solid solution. A minor phase corresponding to Mn during the MA of AlCoCrFeMnNi HEA up to 30 h of milling was also reported by Shivam et al. [134]. Increasing the duration of milling up to 60 h leads to further grain

refinement with no appreciable change in the positions of the peaks. The milling was continued up to 60 h, and it is evident from **Figure 4.2** that the principal diffraction peaks of Mn, namely, (411) (d ~ 2.10 Å), (332) (d ~ 1.90 Å), (422) (d ~ 1.82 Å), (510) (d ~ 1.75 Å) had broadened significantly while the diffraction peaks corresponding to minor reflections, namely, (721), (730), (741) and (831) had almost disappeared. However, after 60 h of milling, a considerable broadening of diffraction peaks was observed due to the enhanced lattice strain and grain refinement. The signature of broadening was most significant, corresponding to the following reflections of Fe: (110) (d ~ 2.03 Å), (200) (d ~ 1.43 Å) and (211) (d ~ 1.17 Å).

Figure 4.2 indicates the presence of two phases in the MgAlMnFeCu HEA, one phase consisting of a BCC solid solution formed by the dissolution of most of the elements along with another phase corresponding to the complex cubic structure close to gamma brass type structure. The lattice parameter of the BCC phase as measured from the XRD pattern, is $a = 2.87 \pm 0.02$ Å, comparable to that of α-Fe, which may appear to act as host lattice. On the other hand, the lattice parameter of γ-brass type phase is $a = 8.92 \pm 0.03$ Å, which is comparable to that of α-Mn (**Table 4.2**). It is evident from the XRD data of **Figure 4.3** that the intensity of the diffraction peaks corresponding to the individual elements decreases accompanied by broadening of the peaks with increasing milling duration. The latter effect is due to a decrease in the crystallite size and an increase in the lattice strain, as given in **Table 4.3**. This increase in lattice strain can be attributed to the fact that elements having atomic radii in the range from 1.27 Å to 1.60 Å are getting accommodated in the host lattice coupled with severe plastic deformation of the powders occurring during the MA process. The formation of two solid solutions, i.e., BCC and γ-brass type phase, which can be considered a solid solution of α-Mn, was complete after 40 h of milling. However, MA was continued up to 60 h to investigate

whether the γ-brass type phase would dissolve into the BCC phase due to continued milling. However, no further phase transformation was observed, nor did the γ-brass type phase entirely dissolve in the BCC phase.

The morphology of 60 h MA HEA is shown in **Figure 4.3 (a-b).** It is observed that the shapes of the MA powder particles are irregular and in size range of 1 to 4 μm. In **Figure 3 (a-b)**, river-like flow patterns are often observed on the surface of the particles, which are a signature of cleavage fracture that may have arisen due to the repetitive cold welding and fracturing of the elemental powders used for making the HEA. The particle size distribution of 60 h milled powder is given in **Figure 4.3 (c),** from which it is evident that the average particle size of the 60 h milled powder is ~ 2.0 ± 0.7μm. The elemental mapping of the 60 h milled MgAlMnFeCu HEA powder sample obtained from SEM-EDS is given in **Figure 4.3 (d-e)**. **Figure 4.3 (d)** shows the targeted powder particle that was analytically mapped for obtaining the chemical composition of the HEA sample.

The chemical composition and EDS spectrum of the HEA powder particle, as obtained from spot-1 in **Figure 4.3(d)** are shown in **Figure 4.3 (e)**. It is evident from the spectrum that the elements are uniformly distributed on a micrometer length scale. The minor variation in chemical composition from the nominal composition may be arising due to variations in the electron beam's interaction volume with particles due to variation in the thickness. The microstructures of the BCC and ϒ-brass type phases were investigated in a detailed fashion using TEM, as shown in **Figure 4.4**. The selected area diffraction (SAD) pattern, corresponding bright-field (BF) and dark field (DF) images predominantly from the BCC phase are shown in **Figure 4.4 (a), (b), (c-d)**, respectively. The SAD patterns indicate the presence of randomly oriented nanocrystalline alloy particles of the two phases mentioned earlier. **Figure 4.4(a)** represents all the reflections corresponding to the BCC and γ-brass type phases, which are also seen in the XRD

patterns in **Figure 4.2**. It can be confirmed that no other intermetallics are detected other than these two phases in the milled samples.

Table 4.1: Composition of phases (atomic fraction) at 300°C, 600°C and 1200°C, calculated using single point calculation tool of Thermo-Calc (SSOL_5 database).

Temp (°C)	Phases	Phase Frac.	Mg	Al	Fe	Mn	Cu
300	BCC_B2#1	0.409	0	0.319	0.423	0.258	0
	Cubic_A13	0.158	0	0.237	0.167	0.595	0
	$CuMg_2$(C15)	0.167	0.667	0	0	0	0.333
	Laves_C15	0.264	0.334	0.120	0	0	0.546
600	BCC_B2#1	0.329	0	0.301	0.421	0.276	0.002
	Cubic_A13	0.225	0	0.246	0.273	0.481	0
	Laves_C15	0.308	0.339	0.143	0	0	0.518
	Liquid	0.137	0.696	0.011	0.003	0	0.288
1200	BCC_B2	0.540	0.001	0.271	0.330	0.368	0.03
	Liquid	0.460	0.433	0.117	0.047	0.002	0.399

The DF image corresponding to (110) reflection of the BCC phase shows the presence of elongated particles forming due to repeated cold welding and fracturing of HEA powder particles. The widely spaced parallel fringes seen in the dark field image in **Figure 4.4(c)** could indicate the presence of planar faults and the appearance of Moire fringes due to the positioning of two crystallites with very similar crystallography. These parallel fringes should not be confused with phase separation. In phase separation, the phases must be interconnected, which is not observed in the present system. The interface between the two phases should be strain-free as both the phases are coherent. From the diffused ring (SADP), it can be understood that phases are not strain-free. Both BCC and γ-brass type phases have fewer slip systems. Thus the formation of planer defects is a

more common phenomenon after 60 h mechanical milling. The appearance of fringes is more likely from the array of planer defects rather than phase separating domain.

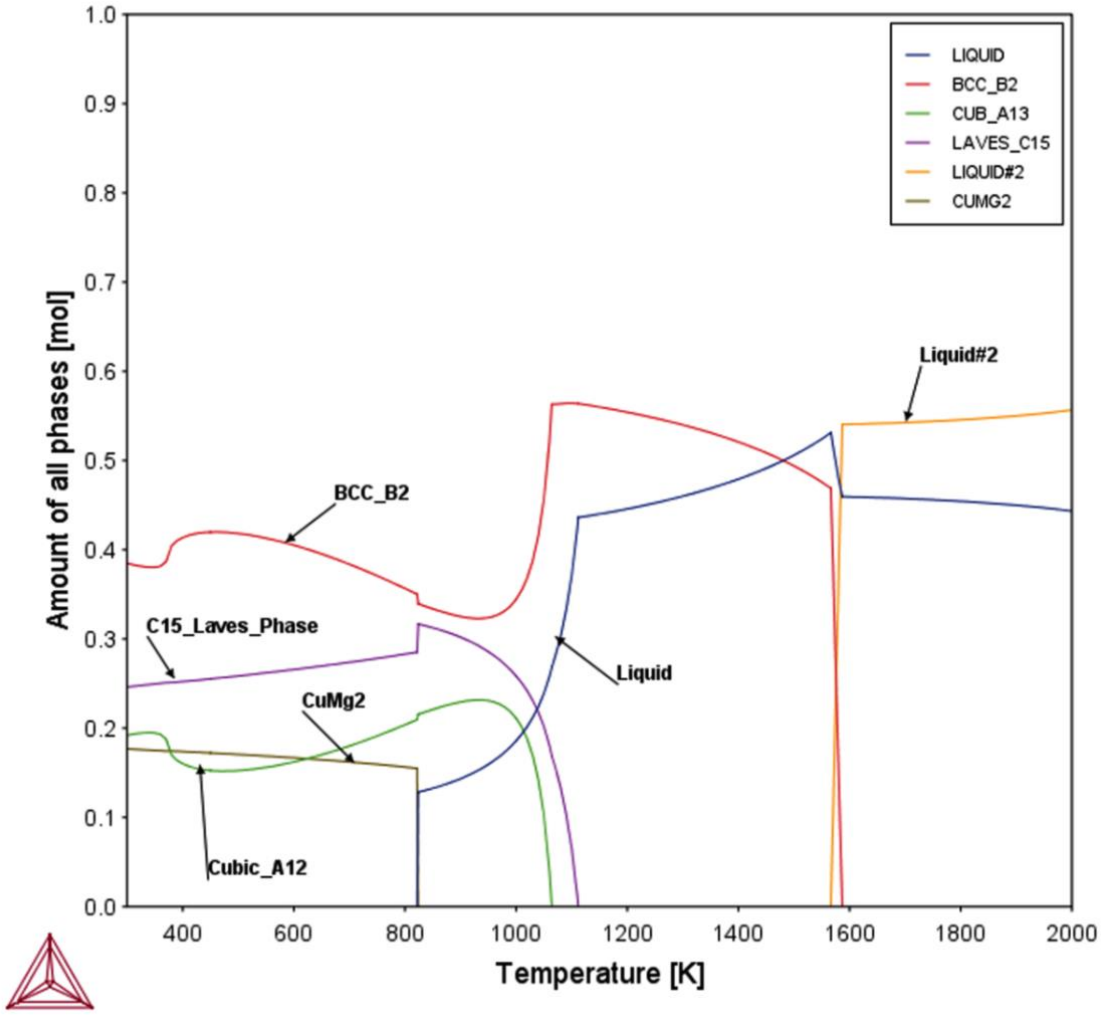

Figure 4.1: Equilibrium diagram calculated by Thermo-Calc using SSOL5 database.

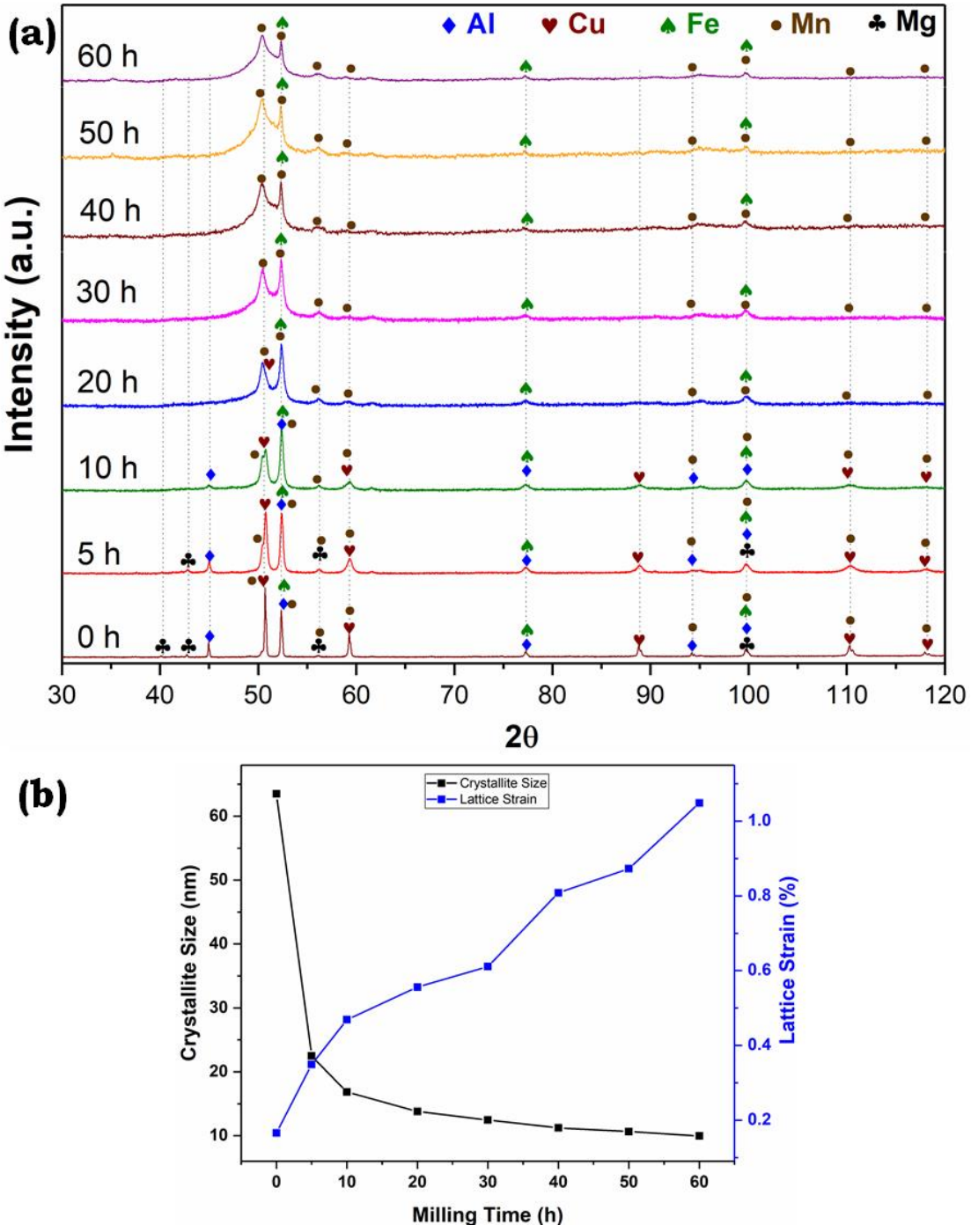

Figure 4.2: (a) Phase evolution during mechanical alloying of MgAlMnFeCu high entropy alloy up to 60 h of MA; (b) variation of crystallite size and lattice strain as a function of milling duration for BCC phase.

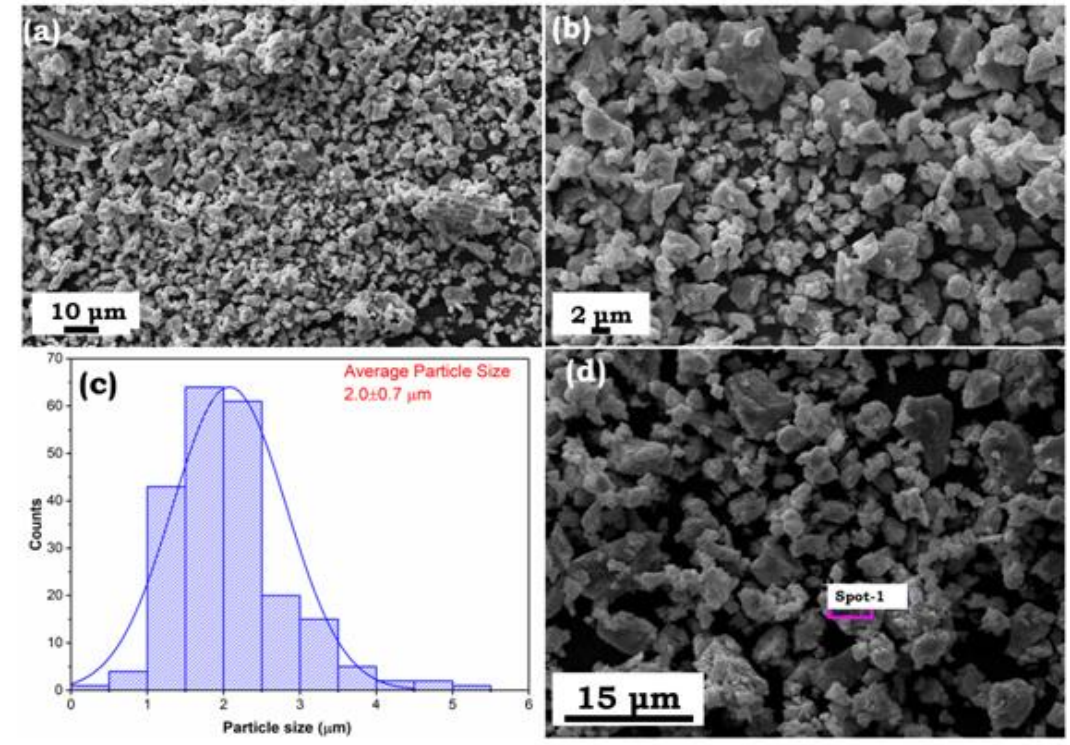

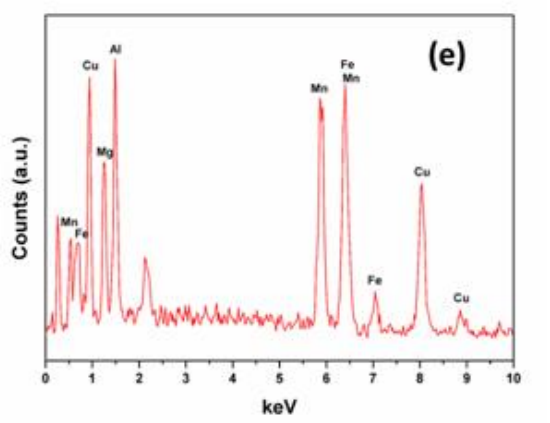

(f)

Element	Atomic%
Mg K	20.16
Al K	19.67
Mn K	18.01
Fe K	19.62
Cu K	22.53

Figure 4.3: SEM micrograph of MgAlMnFeCu HEA MA for 60 h (a) at low magnification showing river like pattern and; (b) at high magnification; (c) particle size distribution of MgAlMnFeCu HEA MA for 60 h; (d) Spot-1 depicting the area used for collecting the chemical composition of HEA MA for 60h; (e) EDS spectrum corresponding to Spot-1 and (f) chemical composition of HEA MA for 60h.

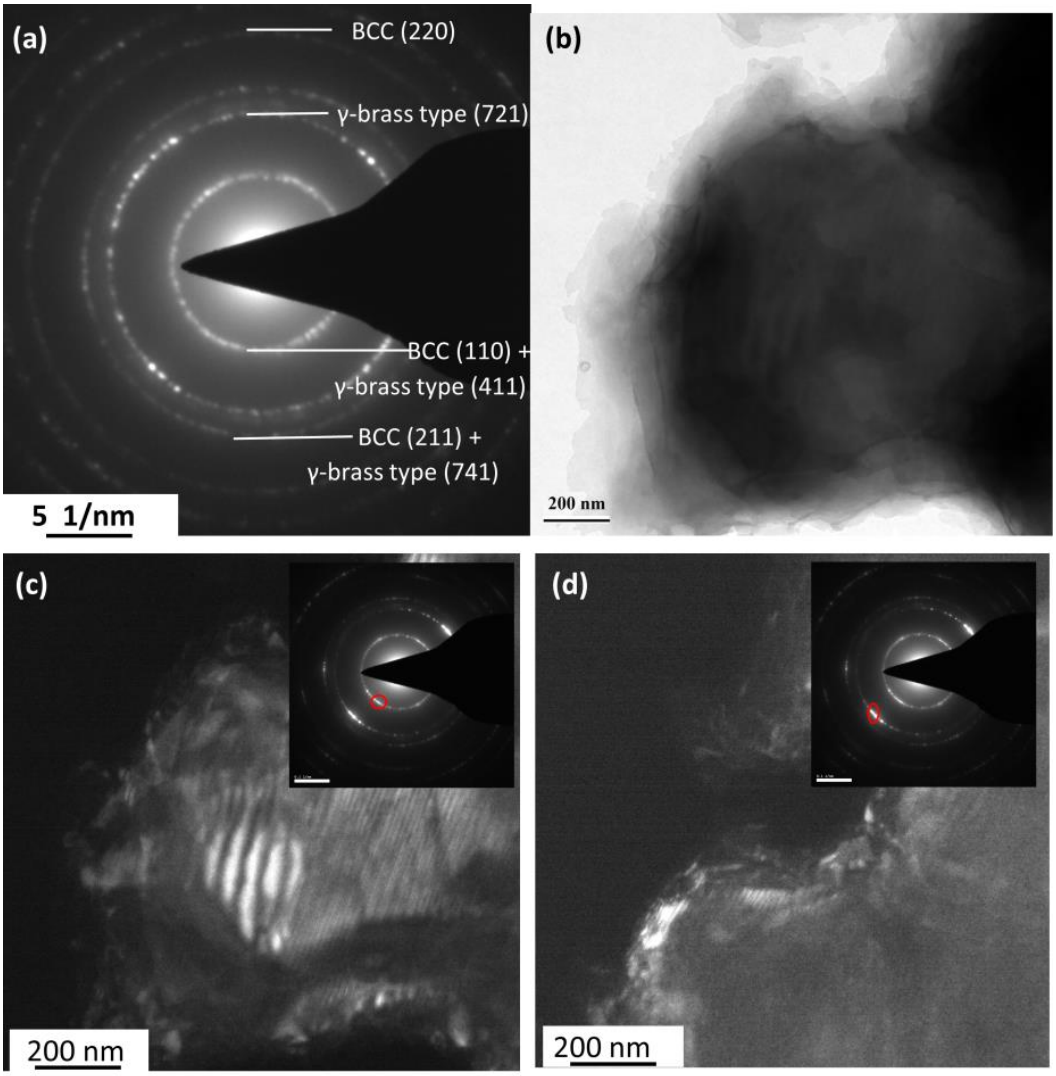

Figure 4.4: (a) Selected area diffraction pattern (SADP) of BCC + γ-brass HEA powder particle; (b) bright-field image corresponding to SADP in figure 3 (a); (c) dark field image of corresponding to BCC (110); (d) dark field image corresponding to γ-brass type (721).

4.3. Thermal stability of as-milled powder of MgAlMnFeCu alloy

The thermal stability of the 60 h milled HEA powder has been investigated using DSC at a heating rate of 50 K min^{-1}, and the corresponding DSC thermogram is shown in **Figure 4.5**. It is evident from the DSC thermogram that there are three exothermic events at T1, T2, and T3 and two endothermic events at T4 and T5. The exothermic event at T1 lies over a large range of temperatures, i.e., ~350 ˚C (623 K) to 450 ˚C (723 K), which

may be attributed to the diffusive transformation of the BCC phase to any complex intermetallic phase. The second exothermic event at T2 occurs at a temperature of 710 ˚C (983 K), which may also be attributed to the diffusive transformation of any complex phase to other intermetallic phases. The nature of this transformation will become clear from the XRD pattern of the powdered sample heat-treated at 400 °C, 600 °C, along with the SPSed HEA sample, as mentioned below. Both of the thermal events may represent a diffusive transformation in nature and start at a lower temperature when the atoms have enough diffusion kinetic energy. However, the kinetics of the transformation becomes fastest at T2. The third exothermic/endothermic event near T3 is seen at a temperature of ~960 ˚C (1233 K) and may be attributed to the partial dissolution of $MgCu_2$ in Υ-brass type phase. An endothermic event T4, seen at a temperature of ~960 ˚C corresponds to the melting of the remaining $MgCu_2$ phase. The fifth and the last thermal event at T5 is endothermic and corresponds to the melting of these equiatomic HEA powder at a temperature of 1170 ˚C (1443 K). Although the thermal events have not been correlated with in-situ XRD data, the phase transformation is predicated on the basis of phase evolution of heat-treated (400 °C, 600 °C) and SPSed HEA powder for 15 min at 900 ˚C (1173 K) as shown in **Figure 4.7-4.9** respectively.

4.4. Characterization of annealed powder of MgAlMnFeCu HEA

Figure 4.6 shows the evolution of phases after annealing the vacuum-sealed (Quartz tube) as-milled powder at 400 °C (673 K) for 2 hrs. The XRD pattern of the heat-treated MgAlMnFeCu HEA shows the formation of $MgCu_2$ and B2 (AlFe-type) intermetallic phases, the diffusive transformation of the BCC phase formed in as-milled condition. $MgCu_2$ ($a = 7.02 \pm 0.02$ Å) is cubic Laves phase (C15) while B2 is a AlFe type phase. The γ-brass type phase present in the as-milled condition is stable up to this temperature.

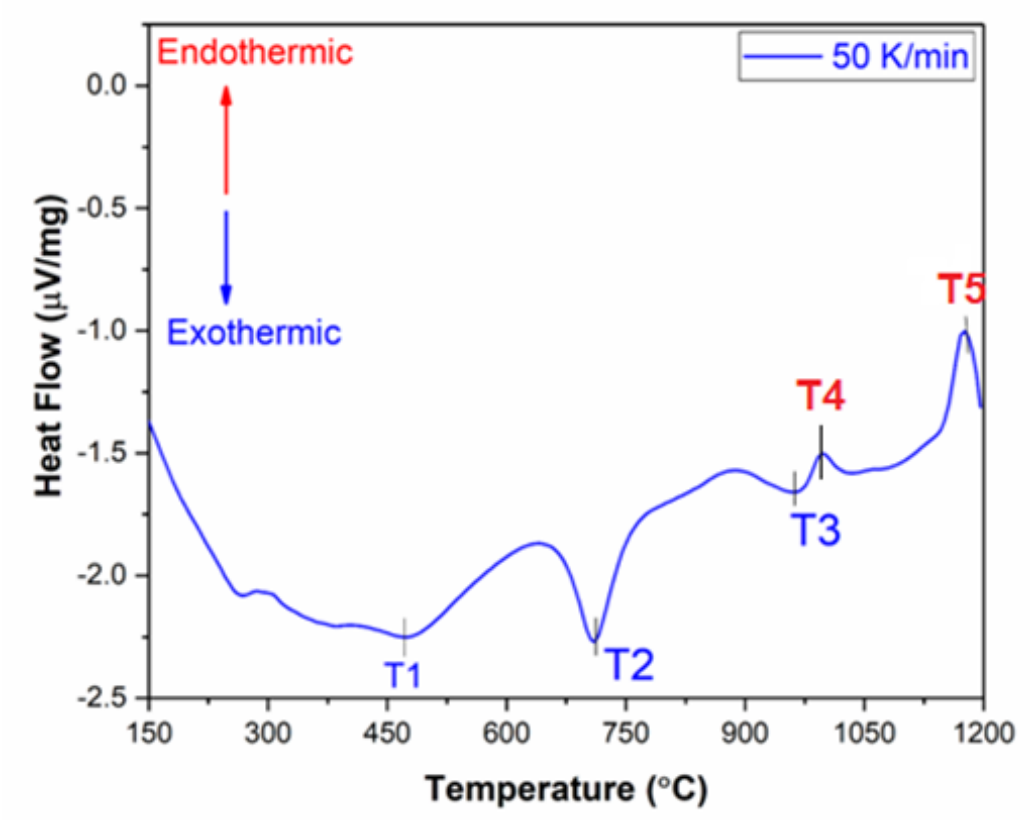

Figure 4.5: DSC thermogram of MgAlMnFeCu HEA MA for 60 h.

Figure 4.7 shows the phases evolved due to the heat treatment of the as-milled HEA powder at 600 °C for 2 hrs. Indexing the XRD peaks shows that all the phases present at 400 °C are intact except for the change in the amount. The volume fraction of the ϒ-brass type phase increases slightly compared to the as-milled condition. Comparing both **Figures 4.6** and **4.7**, we can conclude that the first peak in the DSC thermogram represents a transformation of the BCC phase to $MgCu_2$ type and B2 (AlFe type) intermetallics. At the temperature T1, the diffusive transformation starts. However, the kinetics of the transformation becomes fast at T2. This explains why the shape of the heat event at T1 is shallow and that at T2 becomes quite sharp.

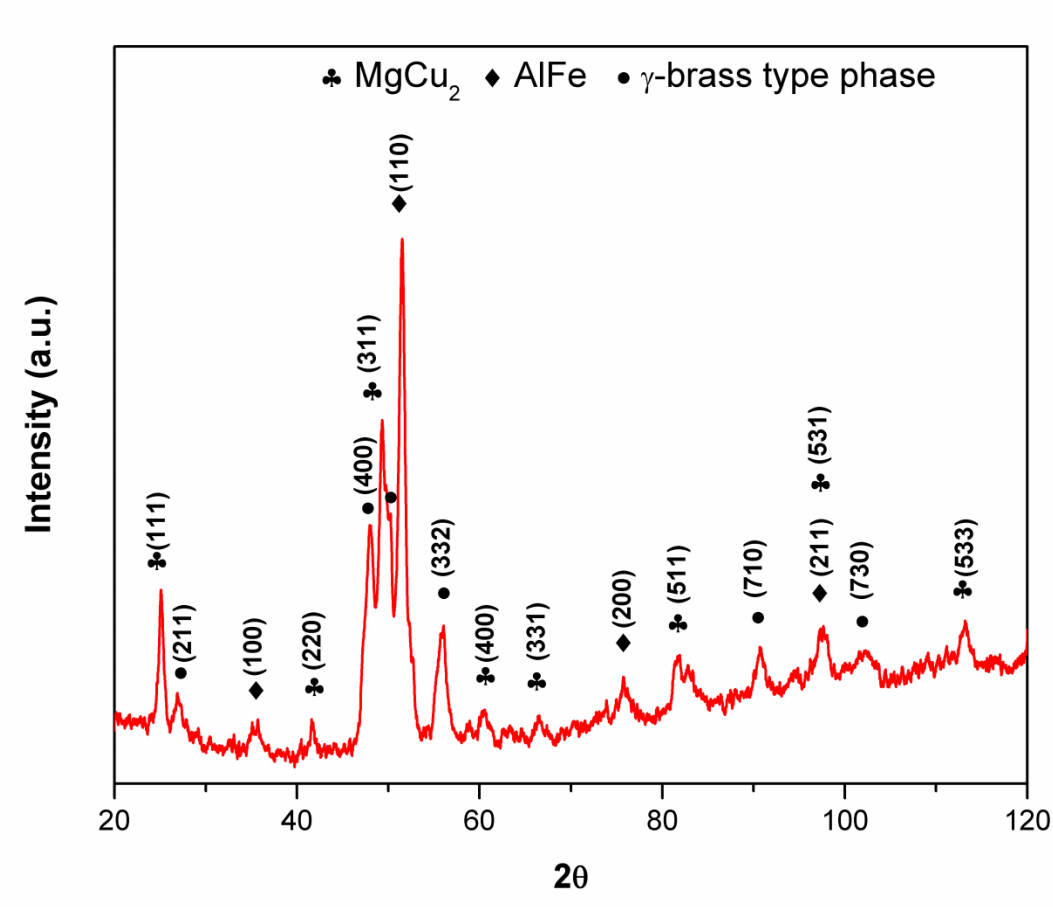

Figure 4.6: Phases evolved in MgAlMnFeCu HEA after heat treating the sample at 400 °C.

4.5. Phase evolution and mechanical properties of SPSed sample

Figure 4.8 shows the evolution of phases after SPS of the 60 h milled MgAlMnFeCu HEA powder at 900 ˚C (1173 K) for 15 min at 50 MPa pressure. The XRD pattern of SPSed MgAlMnFeCu HEA sample in **Figure 4.9** shows the significant reduction in the intensity of the $MgCu_2$ and the increase in the phase fraction of the γ-brass type phase. The enlarged XRD pattern shown in the inset window indicates the co-existence of B2 (AlFe type) and $MgCu_2$ type intermetallic phases along with a significant volume fraction of the γ-brass type phase. The reduction in the amount of $MgCu_2$ in the sample may be due to the melting of the $MgCu_2$ phase having a melting point of 820 °C [135].

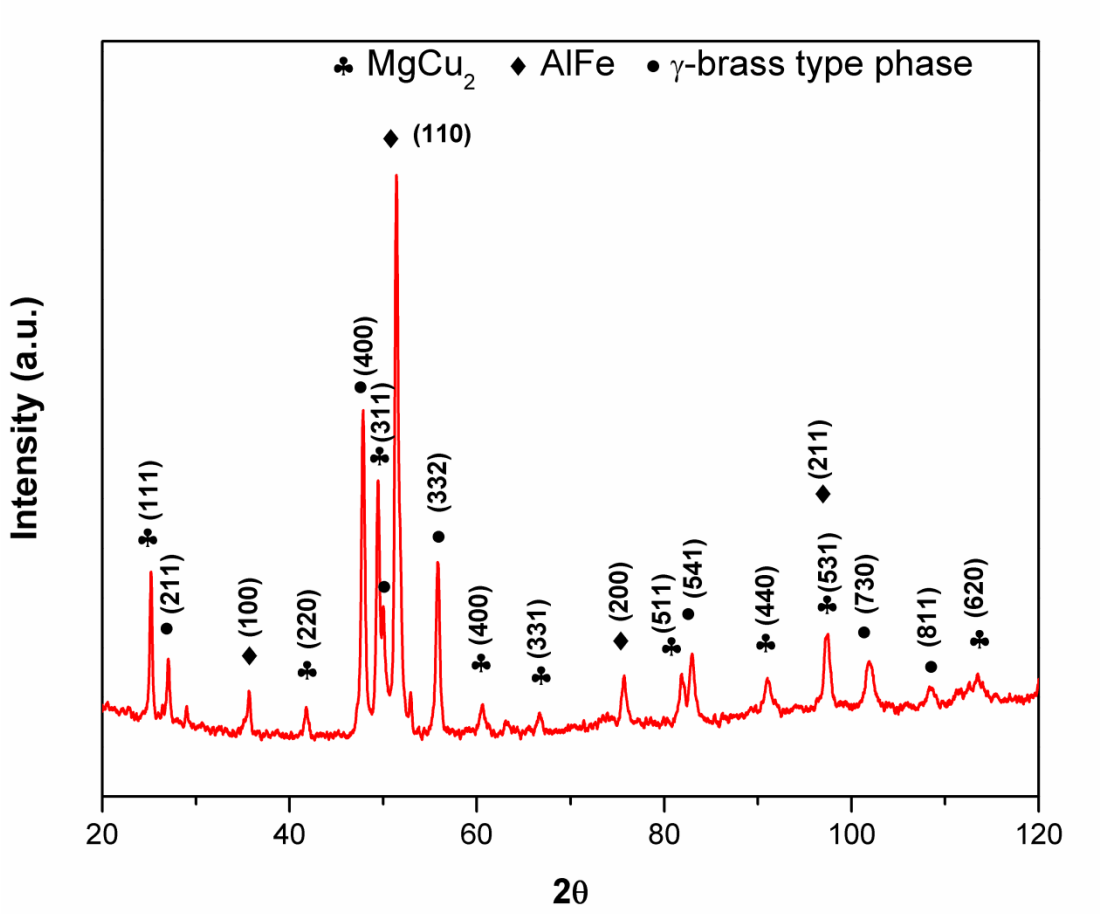

Figure 4.7: Phases evolved in MgAlMnFeCu HEA, heat-treating the sample at 600 °C.

The area selected for the elemental mapping of SPSed HEA is marked in **Figure 4.9 (a)**, while **Figure 4.9 (b)** represents the overall elemental distribution within the selected area of the microstructure. SEM-EDS chemical composition of an individual element within the selected area is shown in **Figure 4.9 (c).** It is evident from **Figure 4.9 (c)** that the bright region in the SPSed MgAlMnFeCu HEA is rich in Mn and Fe and lean in Al, Mg and Cu.

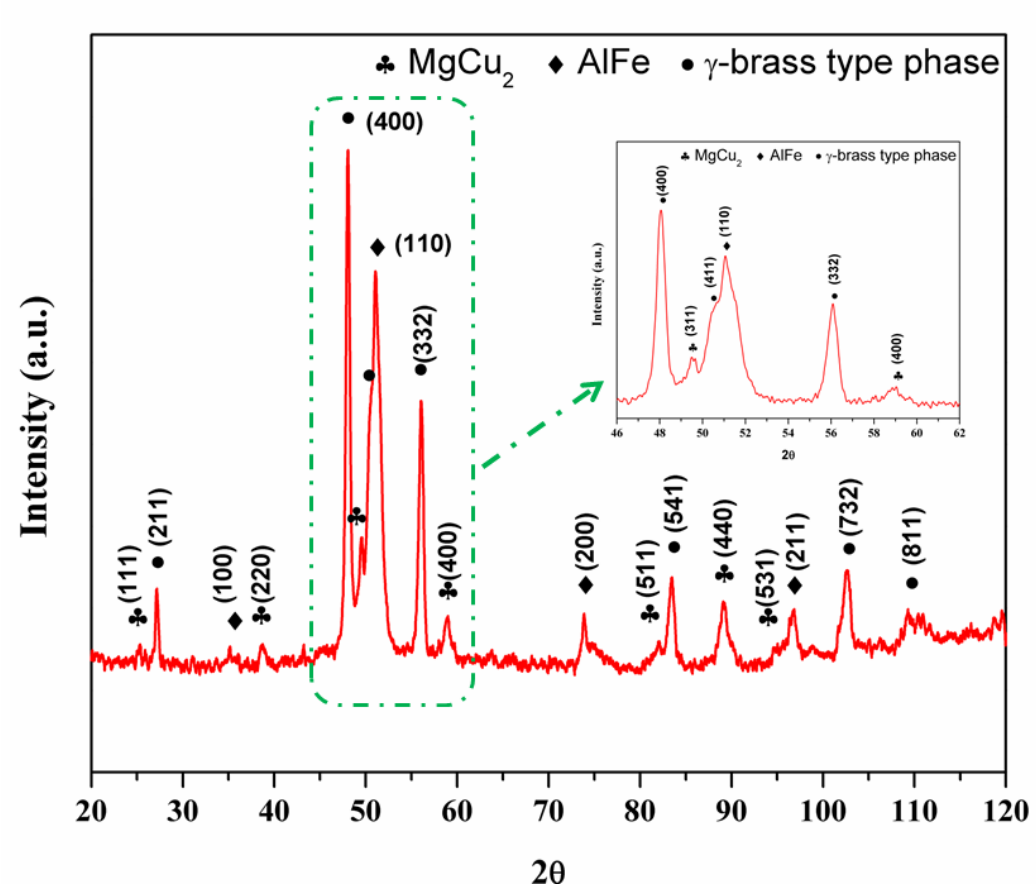

Figure 4.8: Phase evolution of MgAlMnFeCu HEA after SPS; a blown-up image of phase evolved during SPS.

The bulk density, hardness and compressive strength of the MgAlMnFeCu SPSed HEA are reported in **Table 4.4**. It is clear from **Table 4.4** that the relative density of spark plasma sintered HEA is ~ 4.94 g cc^{-1}, which is comparable to that of conventional alloys prepared using the liquid metallurgy route. The density of MgAlMnFeCu HEA with cost-effective alloying elements is better than those of LDHEAs reported in the literature [136]. The bulk hardness and microhardness of these LDHEAs are reported in **Table 4.4**. The microhardness of these alloys was found to be ~ 5.06 GPa with a standard deviation of 0.013 GPa. The hardness of this HEA is even better than that of commercially available alloy systems. The engineering stress vs. engineering strain diagram is shown in **Figure 4.10**, under compressive loading at a strain rate of 1.8 x 10^{-3} s^{-1}. It is clear from

Figure 4.10 and **Table 4.4** that the compressive yield strength and ultimate tensile strength of these alloys have been evaluated to be respectively 1612 MPa and 1792 MPa with very nominal ductility. The failure strain was ~ 6.4% and may be attributed to the brittle nature of the fracture occurring as a consequence of ordered B2 (AlFe type) and $MgCu_2$ type phase formation during sintering.

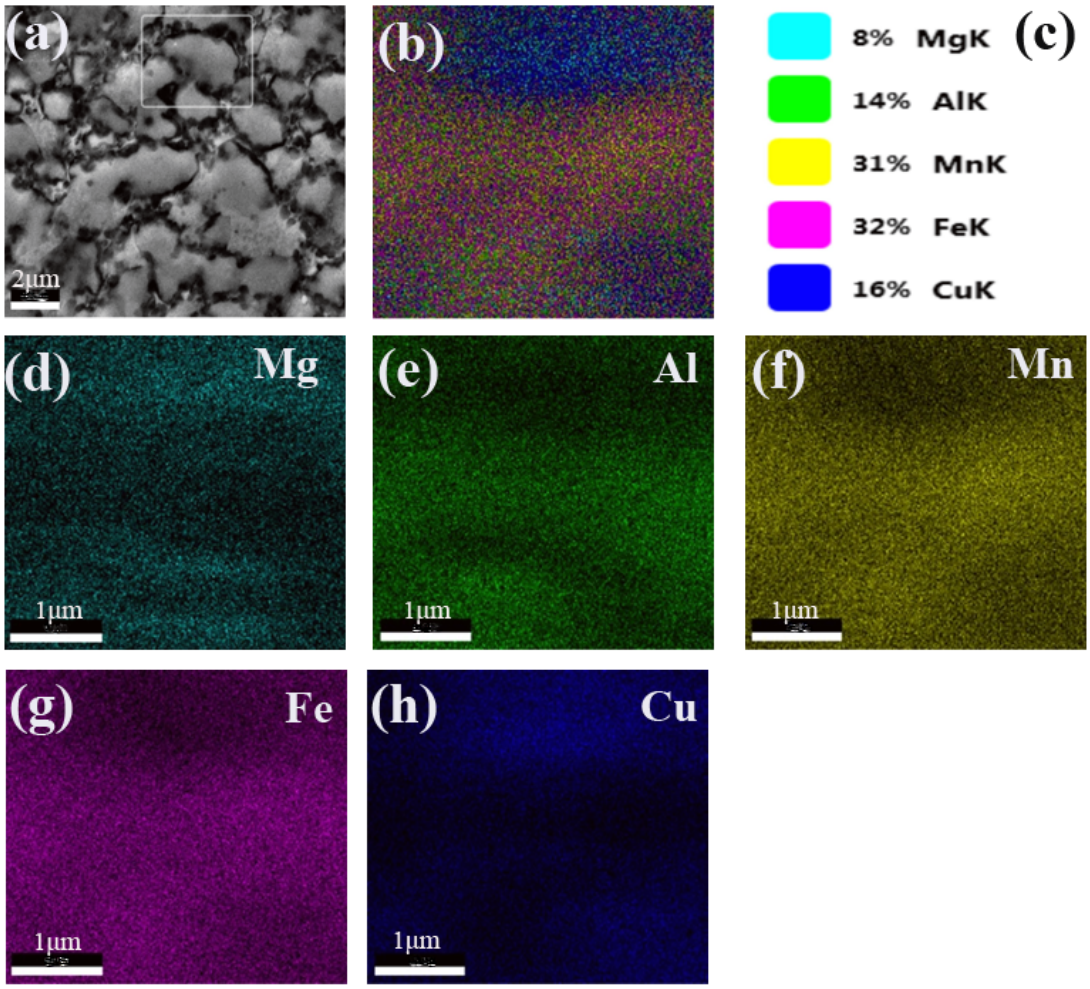

Figure 4.9: SEM micrograph of MgAlMnFeCu (a) spark plasma sintered at 900 ˚C and showing area of elemental mapping; (b) distribution of all the elements within the selected area; (c) SEM-EDS chemical composition of individual elements corresponding to the selected.

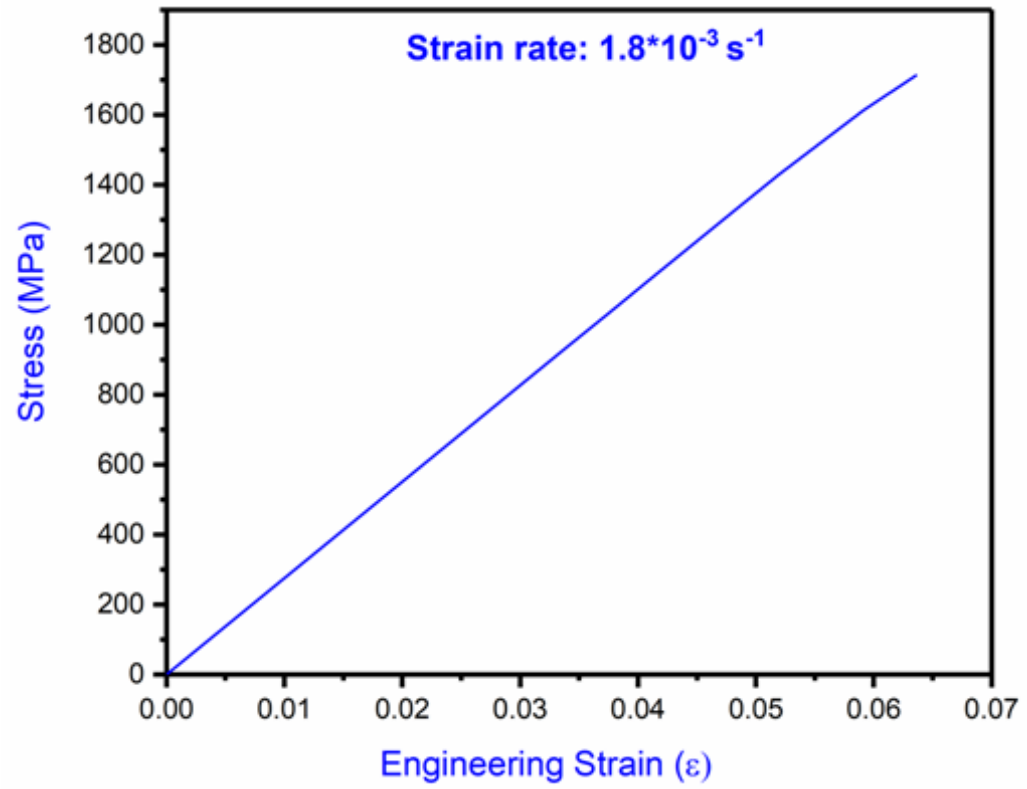

Figure 4.10: Compressive stress-strain plot of MgAlMnFeCu HEA spark plasma sintered at 900˚C for 15 min.

4.6. Discussion

The phase evolution during MA may be explained on the basis of various thermodynamic properties for MgAlMnFeCu HEA. The enthalpy of mixing (ΔH_{mix}) of binary alloy systems of the constituent elements is presented in **Table 4.5**. The enthalpy of mixing for a few binary systems is negative and has a tendency for the formation of intermetallic phases. The highly negative enthalpy of mixing between binary elements such as Al-Fe (−11 kJ mol^{-1}) and Al-Mn (−19 kJ mol^{-1}) [137] favors the formation of intermetallic compounds between these elements and is thermodynamically more favorable. Thus, the major fraction of the microstructure consists of B2 (AlFe type) and ϒ-brass type intermetallic type phase in SPSed samples, which can be seen in **Figures 4.6 and 4.9**. Also, **Table 4.6** shows that MgAlMnFeCu HEA does not satisfy the criteria laid

down by Zhang *et al.* [38] for the formation of a single disordered phase solid solution. Zhang et al. [38] have given three necessary criteria for the formation of single-phase solid solution as (i) $\Delta S_{conf} \geq 13.38$ J $mol^{-1}.K^{-1}$, (ii) –10 kJ $mol^{-1} < \Delta H_{mix} < 5$ kJ mol^{-1}, (iii) $\delta < 6.6\%$. The formation of two phases with different crystal structures despite a comparatively large scatter in the atomic radii of the elements may be due to the presence of high configurational entropy in the HEA. Here, it is important to note that the MgAlMnFeCu HEA system has two elements (Al, Cu) with FCC structure, one (Fe) with BCC structure, one (Mn) with complex cubic structure (close to gamma brass type) and one (Mg) with HCP structure. It is worth mentioning that *α*-Mn has a complex cubic structure, which exhibits various polymorphic transformations as a function of temperature. The initial structure of the phases formed in HEA seems to correspond to that of the constituent elements having higher melting temperatures, namely, Fe and *α*-Mn which serve as host lattices for dissolving the other lower melting elements, as given in **Table 4.2**. Thus, positive enthalpy of mixing and the large atomic size difference (δ) leads to the formation of two solid solution phases α-Fe type BCC and ϒ-brass type phase after MA for 60 h. After doing SPS of prepared HEA, one ϒ-brass type structure along with the formation of B2 (AlFe type) and $MgCu_2$ type intermetallic phases are obtained. In addition to the above-mentioned criteria by Zhang et al. [38], Guo and Liu *et al.* [37] have suggested an additional criterion based on valence electron concentration (VEC) for the formation of a single-phase solid solution. According to this criterion, for VEC > 8.0, 6.87 < VEC < 8.0 and VEC < 6.87 leads to the formation FCC structure, mixture of FCC and BCC structures and BCC structure respectively. Valence electron concentration is calculated as weighted average number of total electrons (including d electrons) present in the valence band of the elements in the alloy. The values of VEC are mentioned in **Table 4.6**, which suggests the likelihood of the formation of BCC crystal structure and is

in line with the criteria suggested by Guo and Liu [37]. Yang and Zhang [48] proposed two criteria for the formation of a single-phase solid solution, namely 'δ' and 'Ω.' For the formation of a single-phase solid solution, the value of δ is less than 6.6% and Ω is greater than 1.1. Although the value of Ω is ~ 6.2, which is well within the above limit, the value of δ is outside the limit, as seen in **Table 4.4**. Therefore, the formation of a single solid solution phase is not expected. In the present investigation, two phases (α-Fe type BCC and ϒ-brass type α-Mn) are present in the HEA after 60 h of milling, while two other intermetallics ($MgCu_2$ type and B2 (AlFe type)) and ϒ-brass type phases were also observed after SPS.

Figure 4.1 display the equilibrium phases that may form at various temperature. At room temperature BCC_B2, Cubic_A13, $CuMg_2$ and $MgCu_2$ type Laves phase are equilibrium phases. There is difference in the results that instead of high temperature β-Mn, as predicted, we have obtained low temperature α-Mn type phase by XRD analysis of the annealed and SPSed sample. As the processing medium was mechanical alloying, where temperature of the powder remains below the transformation of α-Mn to β-Mn structure. If it would have been prepared by melting route than probability of formation of β-Mn will be more. The β-Mn type phase does not appear after annealing may be due to the sluggish diffusion of the elements in the multicomponent alloy. The BCC_B2 phase predicted is Fe-rich phase containing Al and Mn as alloying elements (**Table 4.1**). Thus this phase is in agreement with the experimental results (AlFe type B2 phase). Both $MgCu_2$ and $CuMg_2$ phases are reported by Maulik and Kumar.[138] as predicted by CALPHAD.

The sequence of evolution of phases during milling of MgAlMnFeCu HEA can be summarized as follows:

Pre-mixed elemental powders of Al + Cu + Fe + Mn + Mg (0 h)

→Fe + Mn + Cu + Al + Mg (minor peak disappears) (5h milling)

→Fe + Mn + Cu + Al (significant broadening) + Mg (disappear) (10 h milling)

→Fe + Mn + Cu (significant broadening) + Al (disappear) (20 h milling)

→BCC (Fe) + Complex cubic (Mn) + Cu (disappear) (30 h milling)

→ BCC (Fe) (reduction in crystallite size and increase in strain) + γ-brass type (α-Mn) (disappearance of minor peaks) (60 h milling)

Table 4.2: Physical property of elements in MgAlMnFeCu high-entropy alloy.

	Al	**Cu**	**Fe**	**Mn**	**Mg**
Atomic radius (Å)	1.43	1.28	1.27	1.40	1.60
Melting point (°C)	660	1084	1536	1244	650
Crystal structure	FCC	FCC	BCC	Complex cubic	HCP
Standard lattice parameter (Å)	4.05	3.61	2.86	8.89	a=3.2; c=5.2
Density (g.cm^{-3})	2.70	8.96	7.87	7.40	1.74
Self-diffusion coefficient (m^{2}s^{-1})	10^{-19}	10^{-27}	10^{-31}	10^{-36}	10^{-13}

Table 4.3: The crystallite size and lattice strain for BCC phase of equiatomic MgAlMnFeCu high entropy alloy powder.

Milling Time (h)	**5**	**10**	**20**	**30**	**40**	**50**	**60**
Crystallite size (nm)	23	17	14	12	11	11	10
Lattice strain (%)	0.34	0.46	0.55	0.61	0.81	0.87	1.04

It is evident from experimental results that the MgAlMnFeCu HEA milled for 60 h forms two types of solid solutions as BCC (α-Fe) and Υ-brass type (α-Mn). The sequence of phase evolution is dependent on the physical parameters, as mentioned in **Table 4.2** for the individual elements in the equiatomic composition. The sequence mainly depends upon the melting point, atomic radii and the self-diffusion coefficient. The elements with higher melting points usually act as a host lattice for HEAs as these elements have higher bond strength and stability compared to elements with a low melting point. The self-diffusion coefficient also plays a vital role in dictating the sequence of phase evolution. All the above parameters dictate the sequence of phase evolution during the MA of MgAlMnFeCu HEA. The melting point of Fe is highest among all the other elements used. Similarly, the self-diffusion coefficient of Mg is highest and for Mn, it is lowest. During the systematic investigation of phase evolution during MA of AlCoCrFeMnNi, AlCoCrFeNi and AlCoCrFeNiTi, Shivam *et al.* [134,139,140] have reported the role of the melting point of individual elements for preferential affinity to form host lattice. The sequence mainly depends upon the bond strengths of the elements in the HEA. Similarly, they have also reported the minor phases of Mn along with the Fe and Cr host lattice after completion of MA. In line with the present investigation, Maulik and Kumar [131] have reported the formation of BCC and FCC phases in $AlFeCuCrMg_X$ (x=0, 0.5) HEA. They further reported the formation of two BCC phases with an increase in the mole fraction of Mg (x=1.0, 1.7). Maulik and Kumar [131] also postulated the sequence of phase evolution based on the bond strength as a function of melting point, atomic radii, and self-diffusion coefficient. The self-diffusion coefficient (D) follows the sequence: D(Mn) < D(Fe) < D(Cu) < D(Al) < D(Mg) as mentioned in **Table 4.2**. Although the melting point of Mn is less than that of Fe, it can maintain its identity even after 60 h of MA and accommodating other elements. The SPS

technique achieved the LDHEA with bulk density and relative density of 4.94 g cc-1 and 99.80%. The high hardness and compressive yield strength may be attributed to the solid solution strengthening and precipitation of intermetallics. The present investigation is mainly due to the evolution of AlFe and $MgCu_2$ intermetallic leading to high hardness and compressive yield strength with a failure strain of ~ 6.4%. In literature, an increase in the mechanical properties is mainly attributed to the formation of various intermetallic particles, such as $CuMg_2$, $MgCu_2$, σ- phase corresponding to Fe-Cr and ordered AlFe type phases [131,132]. The hardness and strength of $AlFeCuCrMg_x$ (x= 0, 0.5, 1.0, 1.7) HEA increases with increasing Mg content, as the phase fraction of ordered AlFe increases. However, further investigation is required to improve the ductility and fracture toughness through suitable processing techniques or further alloying addition.

Table 4.4: Density and Compressive strength of MgAlMnFeCu high entropy alloy.

Bulk Density ($g.cm^{-3}$)		**Hardness (GPa)**	**Compressive strength**		
Theoretical density (ρ_{th})	**Experimental Density (ρ_{exp})**	**Microhardness**	**σ(0.2)CYS (MPa)**	**σ_{CUS} (MPa)**	**Failure strain (ε_f)**
4.960	4.946±0.13	5.06 ± 0.013	1612	1792	~6.4%

Table 4.5: Chemical enthalpy of mixing (ΔH_{ij}^{mix} ,$kJ.mol^{-1}$) of atomic pairs for MgAlMnFeCu high entropy alloy, following the Miedema's approach.

Elements	**Al**	**Cu**	**Fe**	**Mn**	**Mg**
Al	-	-1	-11	-19	-2
Cu	-1	-	13	4	-3
Fe	-11	13	-	0	24
Mn	-19	4	0	-	15
Mg	-2	-3	24	15	-

Table 4.6: Calculated thermodynamic and physical parameters of MgAlMnFeCu.

ΔH_{mix} **(kJ.mol^{-1})**	ΔS_{conf} **(J.mol^{-1}K^{-1})**	T_m (K)	Ω	δ (%)	VEC
2.82	13.38	1309	6.2	9.28	6.2

4.7. Conclusions

The present investigation on MgAlMnFeCu LDHEA leads us to the following conclusions.

1. As per the prediction of CALPHAD approach, BCC_B2 is the major phase along with cubic_A13 type and $CuMg_2$ and $MgCu_2$ type Laves phase at lower temperature.
2. Mechanically alloyed MgAlMnFeCu equiatomic powders after 60 h of milling form a mixture of two nanostructured solid solution phases, namely, BCC phase, having lattice parameter close to that of α-Fe structure ($a = 2.87 \pm 0.02$ Å) and γ-brass type phase having lattice parameter close to that of α-Mn ($a = 8.92 \pm 0.03$ Å) type structure which can also be considered as solid solution of α-Mn.
3. The ratio of $-T\Delta S/|\Delta H|$ (i.e., Ω) is ~6.2, which is in the range of solid solution forming HEAs, as reported in the literature. The VEC value of 6.2 for this alloy indicates the formation of a single BCC phase. However, δ (9.2%) acts as the dominating factor, not favouring formation of a single solid solution phase.
4. The HEA is stable up to ~350 °C (623 K), which then undergoes a diffusional transformation of the BCC phase resulting in the B2 (AlFe type) and $MgCu_2$ Laves phases accompanied by the additional γ-brass type phase.

5. Consolidated and spark plasma sintered pellet of this HEA shows high hardness (5.06 GPa) and high compressive yield strength (1612 MPa) at relatively low density (4.94 g cc^{-1}), indicating the possibility of technological applications.